2001-11-15

Three Scanning Techniques for Deep Space Network Antennas to Estimate Spacecraft Position

W. Gawronski

Three Scanning Techniques for Deep Space Network Antennas to Estimate Spacecraft Position

W. Gawronski[1] and E. M. Craparo[2]

Scanning movements are added to tracking antenna trajectory to estimate the true spacecraft position. The scanning movements are composed of harmonic axial movements of an antenna. This scanning motion produces power variations of the received signal, which are used to estimate spacecraft position. Three different scanning patterns (conical scan, Lissajous scan, and rosette scan) are presented and analyzed in this article. The analysis includes evaluation of the estimation errors due to random or harmonic variation of the antenna position and to random and harmonic variations of the power level. Typically, the estimation of the spacecraft position is carried out after completing a full scanning cycle. In this article, sliding-window scanning is introduced, wherein the spacecraft position estimation is carried out in an almost continuous manner, which reduces estimation time by half.

I. Introduction

The NASA Deep Space Network antennas serve as communication tools for space exploration. They are used to send commands to spacecraft and to receive information collected by spacecraft. The spacecraft trajectory (its position versus time) is typically known with high accuracy, and this trajectory is programmed into the antenna, forming the antenna command. However, due to environmental disturbances, such as temperature gradient, gravity forces, and manufacturing imperfections, the antenna does not point precisely towards the spacecraft. These disturbances are difficult or impossible to predict and, therefore, must be measured before compensatory measures can be taken. A technique commonly used for the determination of the true spacecraft position is the conical scanning (conscan) method; see [1–5]. During conscan, circular movements are added to the antenna commanded trajectory, as shown in Fig. 1. These circular movements cause sinusoidal variations in the power of the signal received from the spacecraft by the antenna, and these variations are used to estimate the true spacecraft position.

---

[1] Communications Ground Systems Section.

[2] NASA Undergraduate Student Research Program, Communications Ground Systems Section; student, Massachusetts Institute of Technology, Cambridge, Massachusetts.

The research described in this publication was carried out by the Jet Propulsion Laboratory, California Institute of Technology, under a contract with the National Aeronautics and Space Administration.

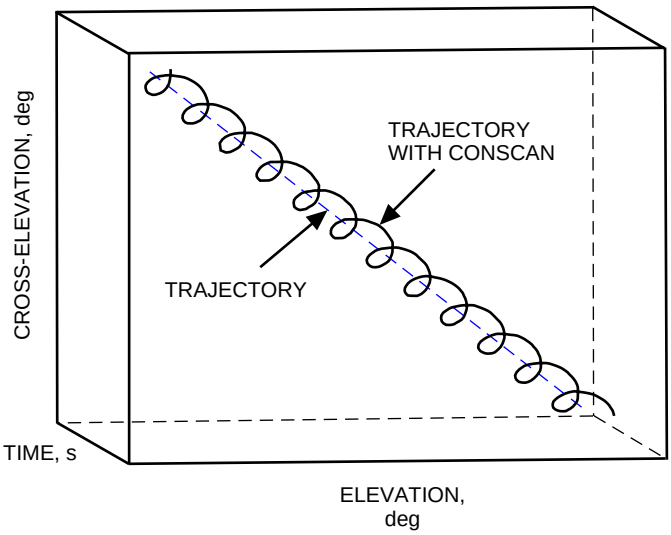

Fig. 1. Schematic diagram of spacecraft trajectory and antenna conscan. The relative size of the conscan radius has been exaggerated.

The radius of the conscan movement is typically chosen such that the loss of the signal power is 0.1 dBi. Thus, the radius depends on the frequency of the receiving signal. For 32-GHz (Ka-band) signals, the conscan radius is 1.55 mdeg. Depending on the radius, sampling rate, antenna tracking capabilities, and desired accuracy, the period of the conscan typically varies from 30 to 120 s (in our case, it will be 60 s). Finally, the sampling frequency was chosen as 50 Hz to match the existing Deep Space Network antenna sampling frequency and to satisfy the Nyquist criterion, which says that the sampling rate shall be at least twice the antenna bandwidth (of 10 Hz).

The conscan technique is used for antenna and radar tracking [1,2]. Descriptions of its use in spacecraft applications can be found in [3–5], and for missile tracking in [6]. Rosette scanning is used in missile tracking [6] and in telescope infrared tracking [7]. This article presents a development of the least-squares and Kalman filter techniques [4,5]. It also introduces and analyzes sliding-window conscan, Lissajous, and rosette scanning, and describes the scans' responses to various disturbances. The notation used in this article is presented in the Appendix.

II. Power Variation during Conscan

Let us begin by defining a coordinate system with its origin located at the antenna command position (i.e., translating with the antenna command). The coordinate system consists of two components: the elevation rotation of the dish and the cross-elevation rotation of the dish. The first component is defined as a rotation with respect to a horizontal axis orthogonal to the boresight, and the second as a rotation with respect to a vertical axis orthogonal to the boresight and elevation axis (see Fig. 2). Since the spacecraft position in this coordinate system is measured with respect to the antenna boresight, and the spacecraft trajectory is accurately known, therefore the position deviations are predominantly caused by either unpredictable disturbances acting on the antenna (e.g., wind pressure) or by antenna deformations (e.g., thermal deformations and unmodeled atmospheric phenomena such as refraction). During conical scanning, the antenna moves in a circle of radius r, with its center located at the antenna command position.

The conscan data are sampled with a sampling frequency of 50 Hz. Thus, the sampling time is $\Delta t = 0.02$ s. The sampling rate was chosen to exceed a doubled antenna bandwidth of 10 Hz. The

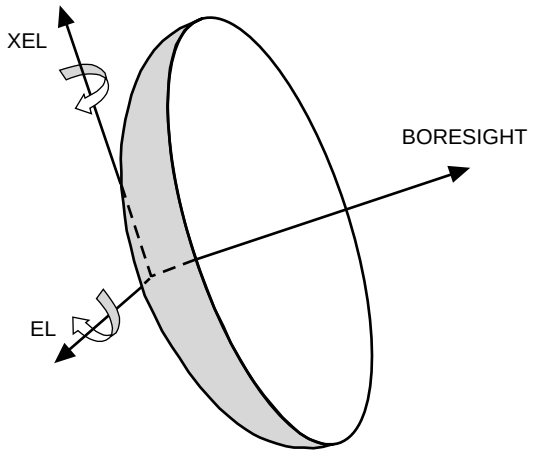

Fig. 2. Elevation and cross-elevation coordinate system.

antenna position a_i at time $t_i = i\Delta t$ consists of the elevation component, a_{ei}, and the cross-elevation component, a_{xi}, as shown in Fig. 3. The position is described by the following equation:

$$a_i = \left\{ \begin{array}{c} a_{eli} \\ a_{xeli} \end{array} \right\} = \left\{ \begin{array}{c} r\cos\omega t_i \\ r\sin\omega t_i \end{array} \right\} \tag{1}$$

Plots of a_{ei} and a_{xi} for $r = 1.55$ mdeg and period $T = 60$ s ($\omega = 0.1047$ rad/s) are shown in Fig. 3.

The target position is denoted by s_i, with the elevation and cross-elevation components denoted by s_{ei} and s_{xi}, respectively (see Fig. 4). The antenna position error is defined as the difference between the target position and the antenna position, i.e.,

$$e_i = s_i - a_i \tag{2}$$

Like the antenna position, it has two components, elevation and cross-elevation position errors:

$$e_i = \left\{ \begin{array}{c} e_{ei} \\ e_{xi} \end{array} \right\} = \left\{ \begin{array}{c} s_{ei} - a_{ei} \\ s_{xi} - a_{xi} \end{array} \right\} \tag{3}$$

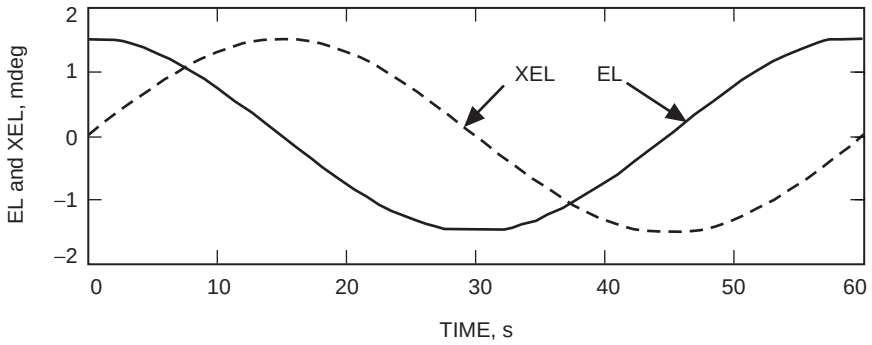

Fig. 3. Elevation and cross-elevation components of conscan.

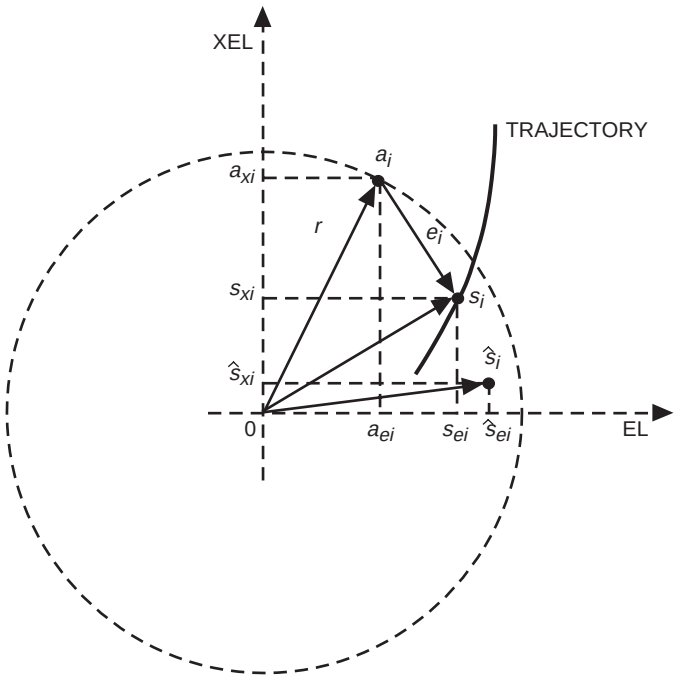

Fig. 4. Antenna position, target position, and estimated target position during conscan.

The total error at $t_i = i\Delta t$ is described as the position rms error, that is,

$$\varepsilon_i = \sqrt{e_i^T e_i} = \|e_i\|_2 \tag{4}$$

Combining Eqs. (1), (2), and (4), one obtains

$$\varepsilon_i^2 = s_i^T s_i - 2a_i^T s_i + a_i^T a_i = s_i^T s_i - 2a_i^T s_i + r^2 \tag{5}$$

Next, we describe how the error impacts the beam power. The carrier power p_i is a function of the error ε_i, and its Gaussian approximation is expressed as

$$p_i = p_{oi} \exp\left(-\frac{\mu}{h^2}\varepsilon_i^2\right) + v_i \tag{6}$$

Note that, although a spacecraft can move relatively quickly with respect to fixed coordinates, it typically moves slowly in the selected coordinate frame (this relative movement is caused by slowly varying disturbances). For example, thermal deformations have a period of several hours, while a conscan period is only 1 minute. Therefore, it is safe to assume that the target position is constant during the conscan period, i.e., that $s_i \cong s$. We also assume that the power is constant during the conscan period, i.e., that $p_{oi} = p_o$.

Using the approximation $\exp(x) \cong 1 + x$, one obtains Eq. (6) as follows:

$$p_i = p_o\left(1 - \frac{\mu}{h^2}\varepsilon_i^2\right) \tag{7}$$

Substituting Eq. (5) into the above equation, and assuming $s_i = s$ and $p_{oi} = p_o$, one obtains

$$p_i = p_o - \frac{p_o \mu}{h^2} \left(r^2 + s^T s - 2 a_i^T s \right) + v_i$$

$$= p_m + \frac{2 p_o \mu}{h^2} a_i^T s + v_i$$

or, using Eq. (1), one obtains

$$p_i = p_m + \frac{2 p_o \mu r}{h^2} \left(s_e \cos \omega t_i + s_x \sin \omega t_i \right) + v_i \tag{8}$$

In the above equations, p_m is the mean power, defined as

$$p_m = p_o \left(1 - \frac{\mu}{h^2} \left(r^2 + s^T s \right) \right) \tag{9}$$

(see [5]). Plots of p_i are shown in Figs. 5 and 6. Additionally, plots of power as a function of antenna position are included in these figures. These plots are presented for the case of the antenna perfectly

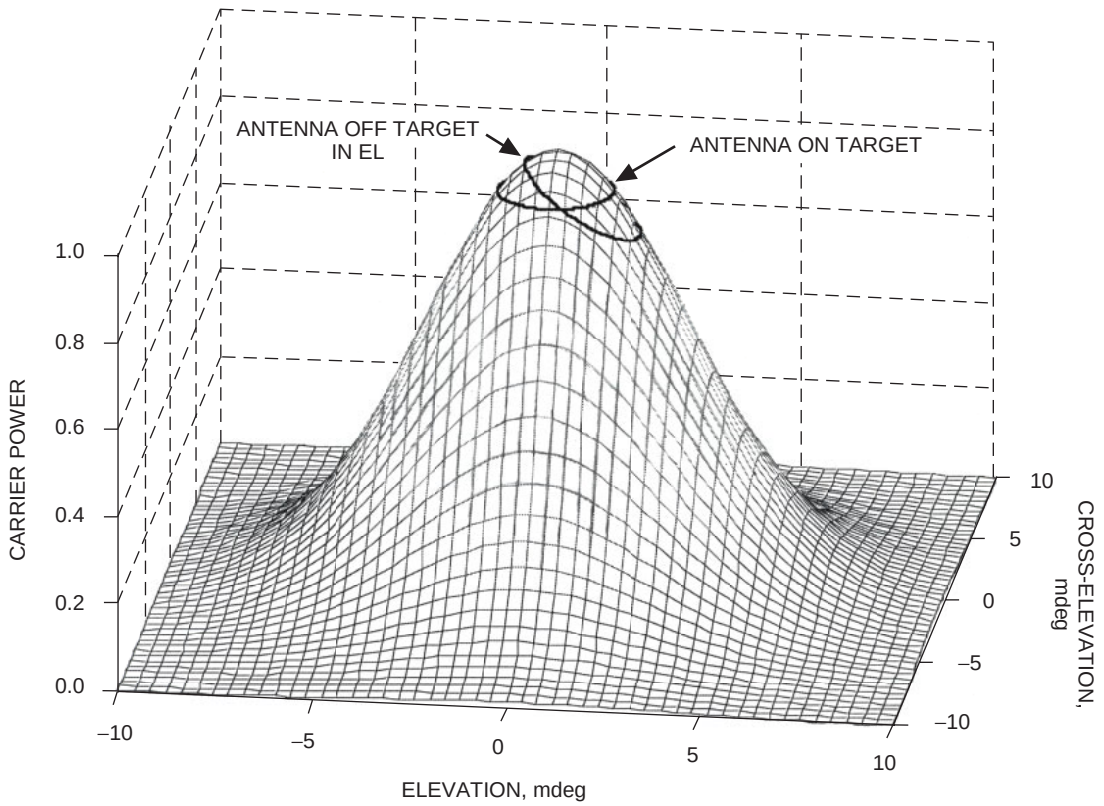

Fig. 5. Carrier power and the conscan power for a perfectly pointed antenna and for elevation error.

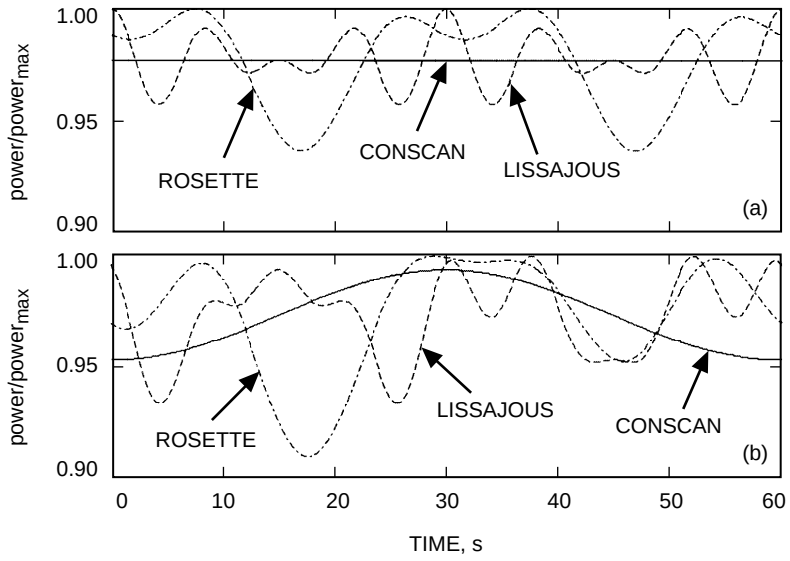

Fig. 6. Power variations (with respect to maximum power) for the conscan, Lissajous, and rosette scans: (a) antenna on target and (b) 0.7-mdeg elevation error.

pointed at the target as well as for the case of an error in antenna elevation. It can be seen that for the perfectly pointed antenna the received power is constant and smaller than the maximum power. For the mispointed antenna, the received power varies in sinusoidal fashion, as derived in the following paragraph.

Equation (9) is a corrected Alvarez algorithm [4]. Here the Taylor expansion was taken with respect to the error ε_i, which produces the maximum power rather than the mean power in the second component in Eq. (8). Denoting the variation from mean power as $dp_i = p_i - p_m$, one obtains from Eq. (8)

$$dp_i = gs_e \cos \omega t_i + gs_x \sin \omega t_i + v_i \tag{10}$$

where

$$g = \frac{2p_o \mu r}{h^2} \tag{11}$$

Here g and ω are known parameters, the power variation dp_i is measured, and the spacecraft coordinates s_e and s_x are to be determined. If no noise were present, the spacecraft position could be obtained from the amplitude and phase of the power variation. Since the received power signal is noisy, the least-squares technique is applied.

III. Estimating Spacecraft Position from the Power Measurements

Denoting

$$k_i = g\,[\cos \omega t_i \quad \sin \omega t_i\,] \tag{12}$$

Eq. (10) can be written as

$$dp_i = k_i s + v_i \tag{13}$$

where $s = \left\{ \begin{array}{c} s_e \\ s_x \end{array} \right\}$. For an entire conscan circle/period,

$$dP = \left\{ \begin{array}{c} dp_1 \\ dp_2 \\ \vdots \\ dp_n \end{array} \right\}, \qquad K = \left[\begin{array}{c} k_1 \\ k_2 \\ \vdots \\ k_n \end{array} \right], \qquad V = \left\{ \begin{array}{c} v_1 \\ v_2 \\ \vdots \\ v_n \end{array} \right\} \tag{14}$$

and Eq. (13) is obtained in the following form:

$$dP = Ks + V \tag{15}$$

The estimated spacecraft position $\hat{s}$ is the least-squares solution of the above equation:

$$\hat{s} = K^{+} dP \tag{16}$$

where $K^{+} = (K^T K)^{-1} K^T$.

IV. Lissajous Scans

In the Lissajous scanning pattern, the antenna position a_i at time $t_i = i\Delta t$ consists of the elevation component, a_{ei}, and the cross-elevation component, a_{xi}, described by the following equation:

$$a_i = \left\{ \begin{array}{c} a_{ei} \\ a_{xi} \end{array} \right\} = \left\{ \begin{array}{c} r \sin n\omega t_i \\ r \sin m\omega t_i \end{array} \right\} \tag{17}$$

where n and m are natural numbers. Again, the components are harmonic functions, which are most desirable for the antenna motion because they do not result in jerks or rapid motions. The Lissajous curve for $r = 1.55$ mdeg, $n = 3$, and $m = 4$ is shown in Fig. 7, and the individual components' plots (a_{ei} and a_{xi}) are shown in Fig. 8. The radius was chosen such that the mean power loss was equal to the mean power loss resulting from a conscan sweep with $r = 1.55$ mdeg.

For this scanning pattern, the power variation is obtained as follows. With the antenna position error defined as in Eq. (2), the total error at $t_i = i\Delta t$ is described as the position rms error:

$$\varepsilon_i^2 = s_i^T s_i - 2a_i^T s_i + a_i^T a_i \tag{18}$$

Using the carrier power p_i as in Eq. (7), and assuming that the spacecraft position and the carrier power are constant during the conscan period, i.e., that $s_i = s$ and $p_{oi} = p_o$, one obtains

$$\begin{aligned} p_i &= p_o - \frac{p_o \mu}{h^2} \left(a_i^T a_i + s^T s - 2a_i^T s \right) + v_i \\ &= p_m \exp\left(\frac{2\mu}{h^2} a_i^T s \right) + v_i \\ &= p_m \exp\left(\frac{2\mu r}{h^2} \left(s_e \sin n\omega t_i + s_x \sin m\omega t_i \right) \right) + v_i \end{aligned} \tag{19}$$

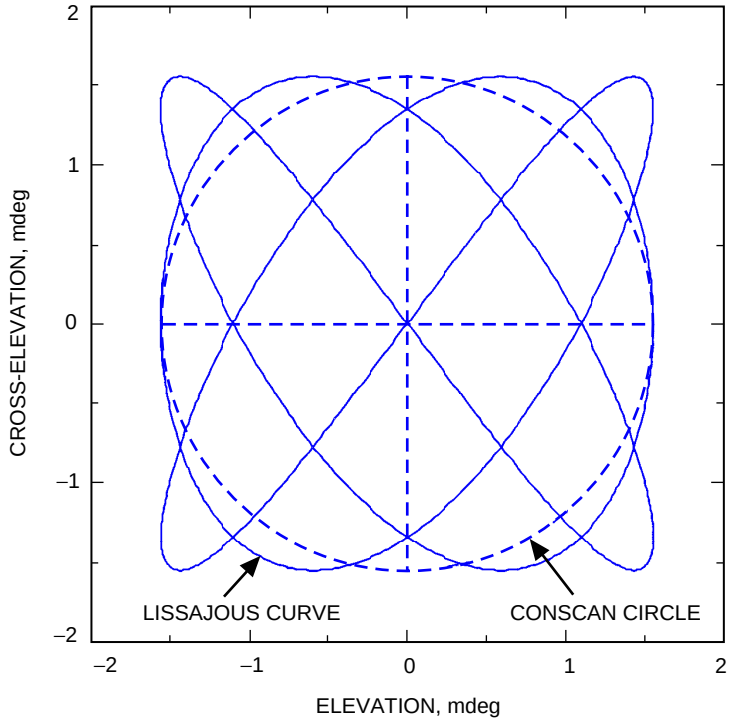

Fig. 7. Lissajous curve for r = 1.55 mdeg, n = 3, and m = 4.

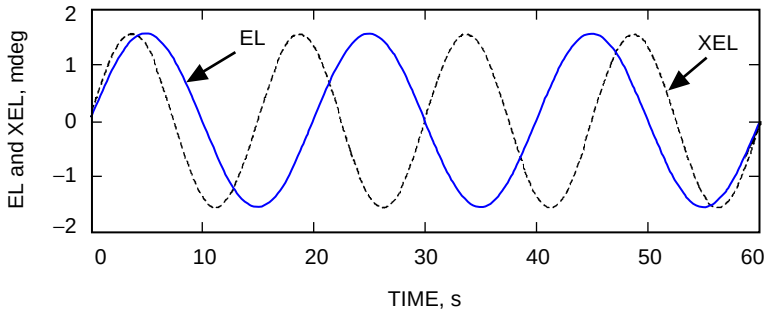

Fig. 8. Elevation and cross-elevation components of the Lissajous scanning pattern for n = 3, m = 4.

Using Eq. (17), one obtains

$$p_i = p_m + \frac{2p_o\mu r}{h^2}(s_e \sin n\omega t_i + s_x \sin m\omega t_i) + v_i \tag{20}$$

where p_m is the mean power, defined as

$$p_m = p_o\left(1 - \frac{\mu}{h^2}\left(a_i^T a_i + s^T s\right)\right) \tag{21}$$

Denoting the variation from mean power as $dp_i = p_i - p_m$, one obtains the power variation as a function of the spacecraft position, s_e and s_x:

$$dp_i = gs_e \sin n\omega t_i + gs_x \sin m\omega t_i + v_i \tag{22}$$

In this equation, g and ω are known parameters, dp_i is measured, and s_e and s_x are spacecraft coordinates to be determined. The plot of the power variation, dp_i, is shown in Fig. 6. It is seen from this figure that power variation occurs even when the antenna is perfectly pointed, unlike the conscan situation. The Lissajous radius, however, was chosen such that on average the loss of the received power is the same as during conscan. Also, unlike the conscan situation, the maximum power is reached during the cycle since the Lissajous curve crosses through the origin.

As in the conscan case, the spacecraft position estimate is obtained from Eq. (16). In the Lissajous case, the matrix K is changed such that its ith row is

$$k_i = g\,[\sin n\omega t_i \quad \sin m\omega t_i\,] \tag{23}$$

V. Rosette Scans

In rosette scanning, the antenna movement is described by the following equation:

$$a_i = \left\{ \begin{array}{c} a_{ei} \\ a_{xi} \end{array} \right\} = \left\{ \begin{array}{c} r\cos n\omega t_i + r\cos m\omega t_i \\ r\sin n\omega t_i - r\sin m\omega t_i \end{array} \right\} \tag{24}$$

The plots of the elevation component, a_{ei}, and the cross-elevation component, a_{xi}, are shown in Fig. 9 for the rosette curve of radius $r = 1.10$ mdeg, $n = 1$, and $m = 3$. The rosette curve itself is shown in Fig. 10 (the radius was chosen such that the mean power loss is the same as for conscan with $r = 1.55$ mdeg). Note that the rosette curve, unlike the conscan circle, crosses the origin and thus receives peak power if the target and boresight positions coincide.

Following the derivation as above, the antenna power is obtained as follows:

$$p_i = p_m + \frac{2p_o\mu r}{h^2}\big(s_e(\cos n\omega t_i + \cos m\omega t_i) + s_x(\sin n\omega t_i - \sin m\omega t_i)\big) + v_i \tag{25}$$

Therefore, the power variation is

$$dp_i = gs_e(\cos n\omega t_i + \cos m\omega t_i) + gs_x(\sin n\omega t_i - \sin m\omega t_i) + v_i \tag{26}$$

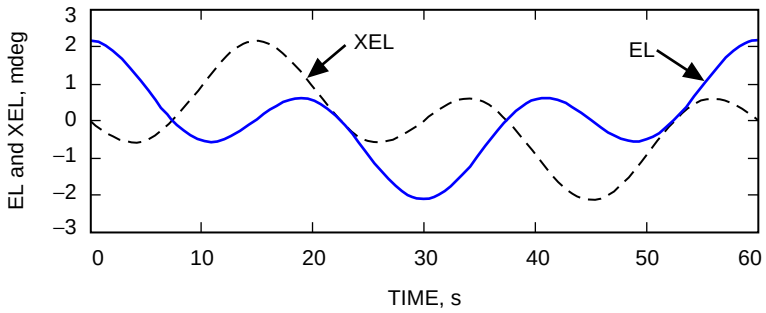

Fig. 9. Rosette elevation and cross-elevation components.

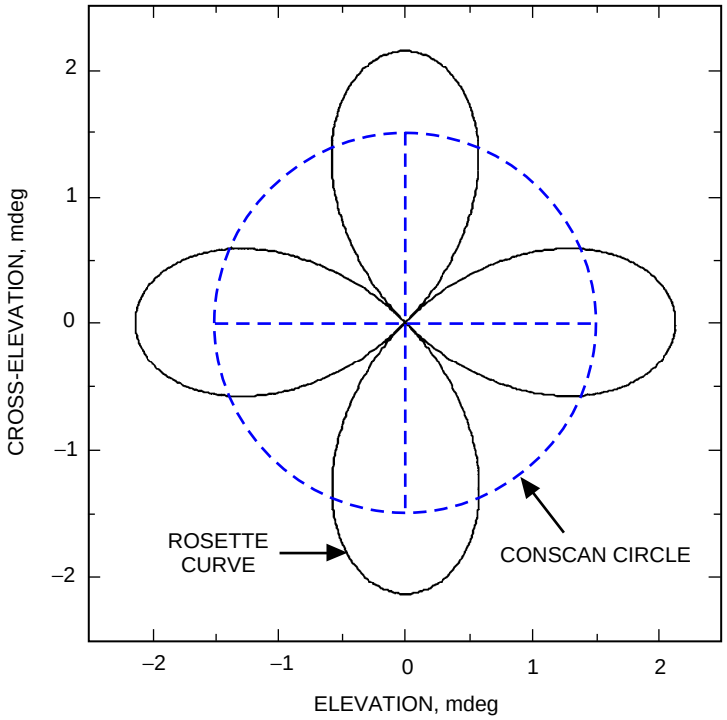

Fig. 10. Rosette curve for r = 1.1 mdeg, n = 1, and m = 3.

where g is given by Eq. (11). The plots of variations of dp_i are shown in Fig. 6. The plots show that received power varies for the perfectly pointed antenna. Also, like the Lissajous case, the maximum power is reached during the cycle, since the rosette curve crosses through the origin.

The spacecraft position estimate is determined from the above equation, using Eq. (16), where the ith row of the matrix K in this equation is

$$k_i = g\left[\cos n\omega t_i + \cos m\omega t_i \quad \sin n\omega t_i - \sin m\omega t_i\right] \tag{27}$$

VI. Performance Evaluation

The scanning performance is evaluated in the presence of disturbances. First, the antenna position is disturbed by random factors, such as wind gusts, and by deterministic disturbances, which can be decomposed into harmonic components. Secondly, the carrier power is also modeled as disturbed by random noise (receiver noise, for example) and deterministic variations, such as spacecraft spinning. The latter disturbances are decomposed into harmonic components.

A. Position Disturbances

Position disturbances are caused by antenna motion. These disturbances may be purely random, and as such modeled as white Gaussian noise of a given standard deviation, or more or less deterministic disturbances, which are modeled as harmonic components within a bandwidth up to 10 Hz (i.e., antenna dynamics bandwidth).

The random disturbances were simulated separately in the elevation and cross-elevation directions. The estimation errors due to disturbances are shown in Tables 1 and 2, respectively. They show that the scanning algorithms have quite effective disturbance-rejection properties. In conscan, for example, a disturbance in the cross-elevation direction of 0.3-mdeg standard deviation will cause approximately 0.005 mdeg of error in the elevation estimation and 0.01 mdeg of error in the cross-elevation estimation.

The antenna position x_a was also disturbed by a harmonic motion in the elevation direction of frequency f and amplitude 0.1 mdeg. The disturbance's impact on estimation accuracy was analyzed for frequencies ranging from 0.0001 Hz (very slow motion) to 10 Hz (antenna bandwidth). Note that the scanning frequency is $f_o = 1/60 = 0.0167$ Hz. Consider the plots of the estimation error in elevation and cross-elevation as shown in Figs. 11(a) and 11(b). They show that for frequencies higher than the scanning frequency the disturbances are quickly suppressed. The slope of the error magnitude drops as follows: for conscan, -60 dB/dec in elevation and -40 dB/dec in cross-elevation; for Lissajous scans, -20 dB/dec in elevation and -60 dB/dec in cross-elevation; and for rosette scans, -20 dB/dec in elevation and -40 dB/dec in cross-elevation. For low frequencies, the disturbance level is constant in elevation for all scans and drops down in cross-elevation: -20 dB/dec for conscan and rosette scanning, and -40 dB/dec for Lissajous scanning.

When the harmonic disturbance is applied in cross-elevation, the picture is symmetric: whatever was said previously about estimation error in elevation is now true for cross-elevation and vice versa.

Table 1. Estimation error due to unit noise, mdeg, in elevation.

Direction	Conscan, mdeg	Lissajous, mdeg	Rosette, mdeg
Elevation	0.025	0.025	0.037
Cross-elevation	0.013	0.017	0.010

Table 2. Estimation error due to unit noise, mdeg, in cross-elevation.

Direction	Conscan, mdeg	Lissajous, mdeg	Rosette, mdeg
Elevation	0.015	0.019	0.010
Cross-elevation	0.027	0.029	0.037

B. Power Disturbances

Random power variation was also simulated. Variations had standard deviations ranging from 0.1 to 10 percent of maximum power. For all three scans, the elevation and cross-elevation estimation error were proportional to the variation of power with a gain of 0.080–0.089 mdeg per 10 percent of power variation, as shown in Table 3. This is very effective suppression of power noise, since the 10 percent standard deviation of power variation causes less than 0.1-mdeg estimation error.

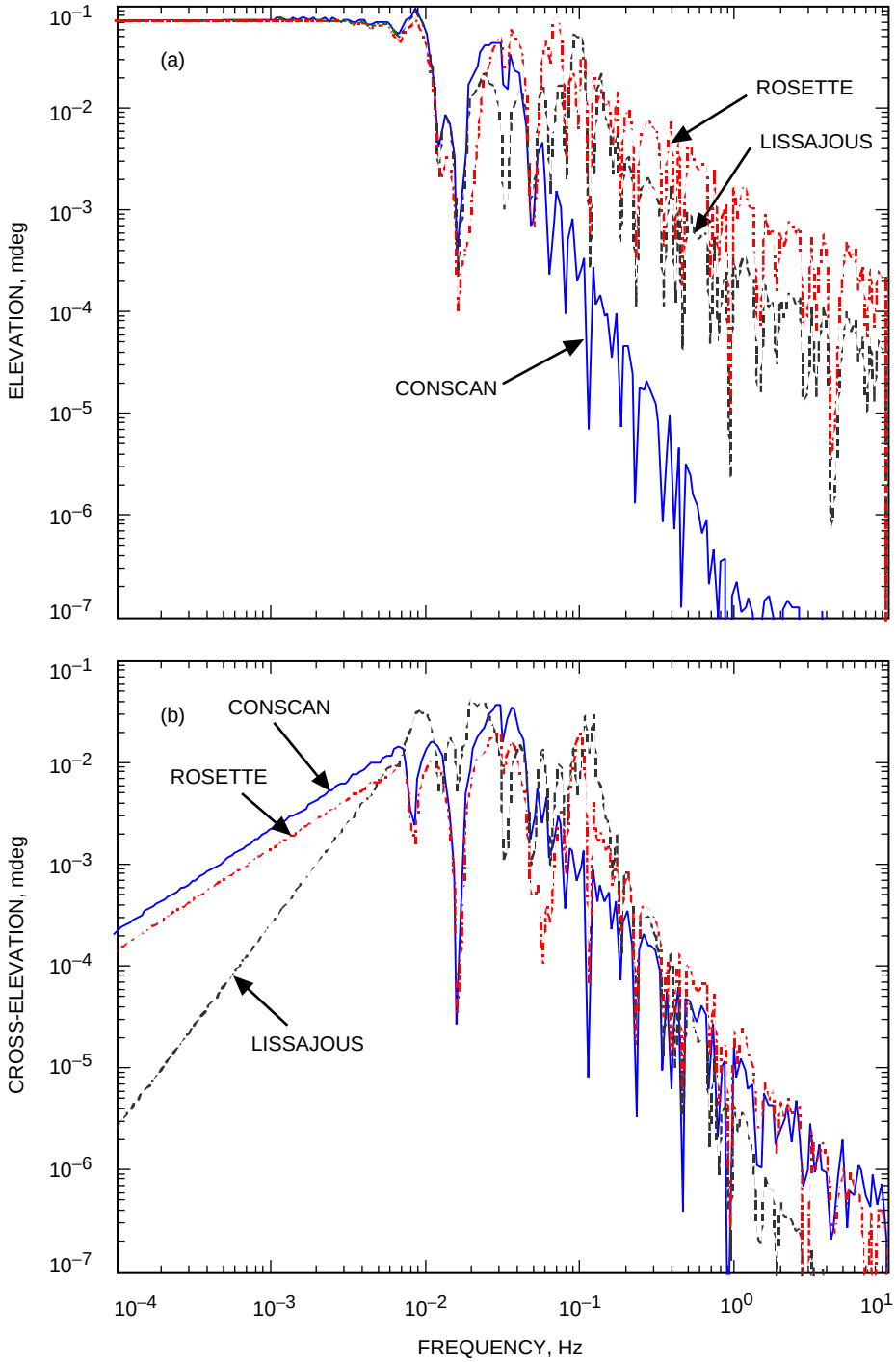

Fig. 11. Estimation errors in response to an elevation harmonic disturbance of amplitude 0.1 mdeg: (a) elevation error and (b) cross-elevation error.

Table 3. Estimation error due to power noise. The standard deviation of the power noise is 10 percent of peak power.

Direction	Conscan, mdeg	Lissajous, mdeg	Rosette, mdeg
Elevation	0.089	0.083	0.080
Cross-elevation	0.089	0.080	0.088

Next, the impact of pulsating power on the estimation of the elevation and cross-elevation positions was analyzed. The results are shown in Figs. 12(a) and 12(b). The harmonic power variations were of frequencies ranging from 0.0001 Hz to 10 Hz, and of amplitude 0.1 (10 percent of maximal power). The plots show that the maximal estimation error of 3-mdeg amplitude was observed for frequencies near the scan frequency, and that for lower and higher frequencies the amplitude of the estimation errors quickly drops. Thus, all three scanning algorithms act as effective filters for this kind of disturbance.

VII. Sliding-Window Conscan

The spacecraft position estimation technique described up to this point has used data collected during a single scanning period. Thus, the spacecraft position estimate is updated every period T, which typically ranges from 60 to 120 s. This is a rather slow update that can cause a significant lag in the antenna tracking if the assumption of slowly varying target position is incorrect. This lag can be improved using a technique known as sliding-window scanning. In sliding-window scanning, spacecraft position is estimated every time period ΔT, where $\Delta T < T$. The update moments are shown in Fig. 13 for $\Delta T = (1/3)T$. In this case, the data used in Eq. (15) do not start at the beginning of every circle; rather, they begin at times T, $T + \Delta T$, $T + 2\Delta T$, $T + 3\Delta T$, etc. Note that the first estimation is at T rather than ΔT because an entire circle is required to complete the estimation process. The data are collected for an entire circle, as shown in Table 4.

To see the usefulness of the sliding-window technique in the estimation process, assume that the target position changes rapidly by 0.15 mdeg at $t = 150$ s. This type of shift may be caused by a sudden disturbance in antenna position, such as a large gust of wind. This is an extreme situation, since in the closed-loop configuration the control system would "soften" the impact of the gusts. The shift is illustrated in Fig. 14, along with simulated responses of antennas using the traditional conscan method and the sliding-window method. The simulations show that, for the conscan period $T = 60$ s, 120 s are required to reach the target, whereas the sliding-window conscan with $\Delta T = 5$ s reaches the target in half the time, i.e., in 60 s. This is especially important when antenna dynamics are involved, since faster sensors improve the pointing accuracy. Similar results were obtained for the Lissajous and rosette scans.

VIII. Conclusions

Three scanning techniques (conical, Lissajous, and rosette scans) were analyzed. It was shown that all of them have similar properties in the estimation accuracy of the spacecraft position for random and harmonic disturbances. Therefore, where the spacecraft angular position is concerned, conscan should be chosen due to its simplicity of implementation. Sliding-window scans were introduced and analyzed, and it was shown that they are significantly faster than non-sliding scans while preserving other non-sliding scan properties.

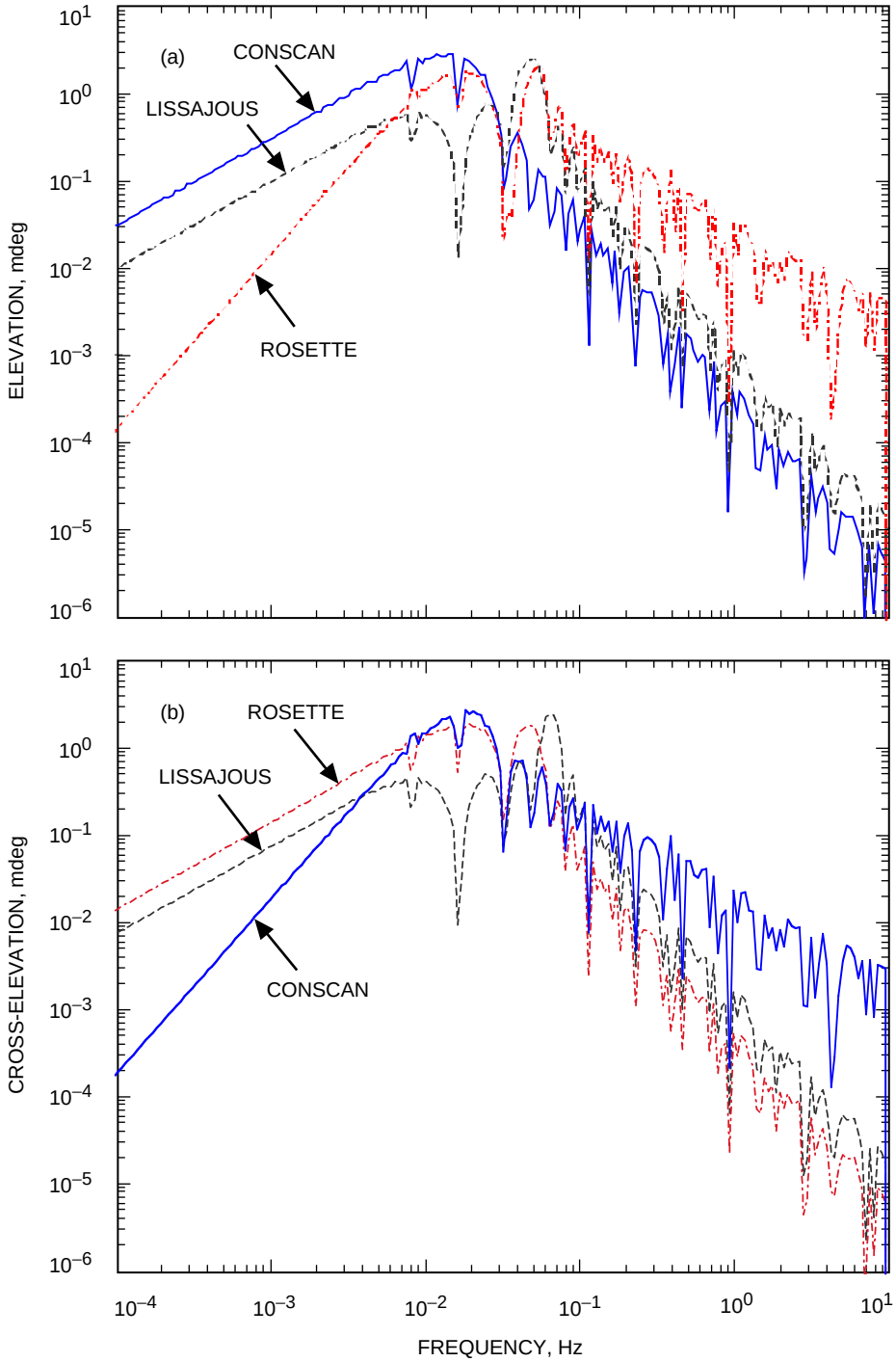

Fig. 12. Estimation errors in response to harmonic power variation: (a) elevation error and (b) cross-elevation error.

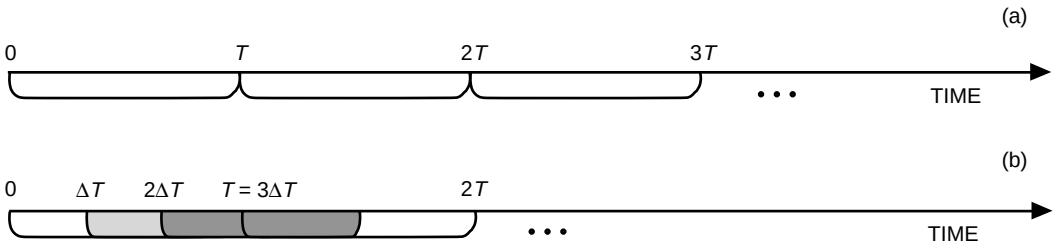

Fig. 13. Scans with the (a) non-sliding and (b) sliding-window techniques, for $\Delta T = (1/3)T$.

Table 4. Data collection time for the sliding-window scan.

Data collection time	Time span of the circle
T	$[0, T]$
$T + \Delta T$	$[\Delta T, T + \Delta T]$
$T + 2\Delta T$	$[2\Delta T, T + 2\Delta T]$
$T + i\Delta T$	$[i\Delta T, T + i\Delta T]$

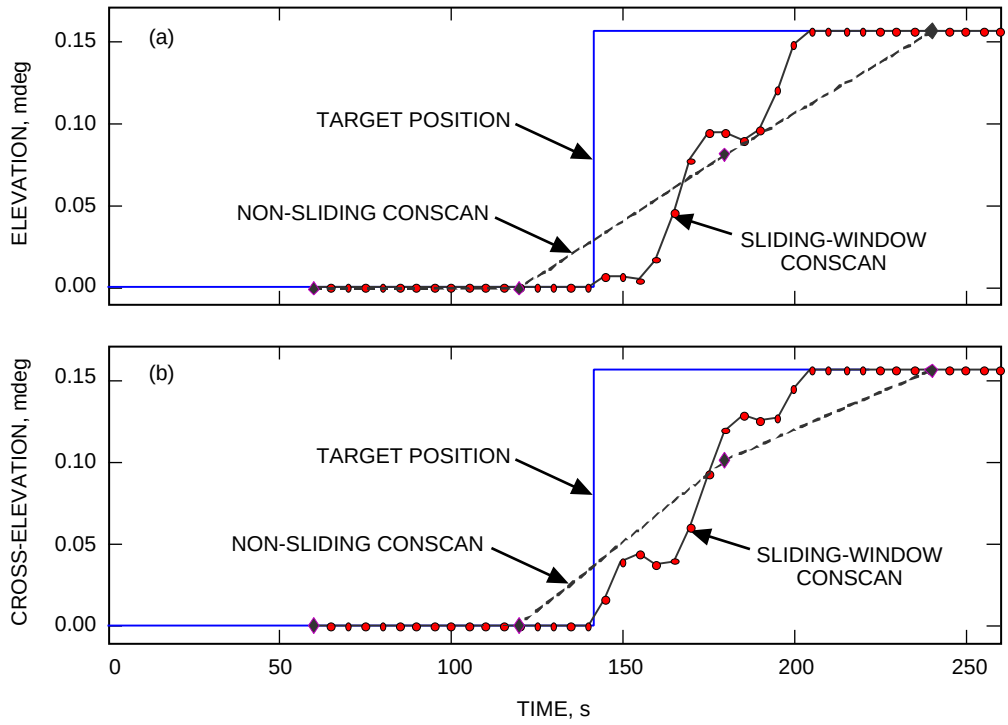

Fig. 14. Estimated spacecraft position for sliding-window conscan and non-sliding conscan: (a) elevation and (b) cross-elevation.

The algorithms presented here are based on the least-squares conscan algorithm by Alvarez [4] and the Kalman algorithm by Eldred [5]. It should be noted that the two algorithms are similar, since both result from the assumption of negligibility of the spacecraft movement with respect to the antenna position during the conscan period. It is a justified assumption, but the Kalman algorithm in this case becomes a least-squares algorithm. It is also worth noting that the Alvarez algorithm, unlike the Eldred algorithm, estimates the peak power of the signal in addition to the spacecraft position, but because there is interdependence between the power and spacecraft position, this algorithm can produce biased results.

References

[1] J. B. Damonte and D. J. Stoddard, "An Analysis of Conical Scan Antennas for Tracking," *IRE National Convention Record*, vol. 4, pt. 1, pp. 39–47, 1956.

[2] G. Biernson, *Optimal Radar Tracking Systems*, New York: Wiley, 1990.

[3] J. E. Ohlson and M. S. Reid, *Conical-Scan Tracking with 64-m Diameter Antenna at Goldstone*, JPL Technical Report 32-1605, Jet Propulsion Laboratory, Pasadena, California, October 23, 1976.

[4] L. S. Alvarez, "Analysis of Open-Loop Conical Scan Pointing Error and Variance Estimators," *The Telecommunications and Data Acquisition Progress Report 42-115, July–September 1993*, Jet Propulsion Laboratory, Pasadena, California, pp. 81–90, November 15, 1993.
http://tmo.jpl.nasa.gov/tmo/progress_report/42-115/115g.pdf

[5] D. B. Eldred, "An Improved Conscan Algorithm Based on a Kalman Filter," *The Telecommunications and Data Acquisition Progress Report 42-116, October–December 1993*, Jet Propulsion Laboratory, Pasadena, California, pp. 223–231, February 15, 1994.
http://tmo.jpl.nasa.gov/tmo/progress_report/42-116/116r.pdf

[6] H.-P. Lee and H.-Y Hwang, "Design of Two-Degree-of-Freedom Robust Controllers for a Seeker Scan Loop System," *Int. Journal of Control*, vol. 66, no. 4, pp. 517–538, 1997.

[7] H. Wan, Z. Liang, Q. Zhang, and X. Su, "A Double Band Infrared Image Processing System Using Rosette Scanning," *Detectors, Focal Plane Arrays, and Applications, SPIE Proceedings*, vol. 2894, pp. 2–10, 1996.

Appendix

Notation

Ka-band= 32 GHz

EL = elevation

XEL = cross-elevation

dBi = dB power relative to isotropic source

Δt = sampling time ($\Delta t = 0.02$ s)

i = sample number

$t_i = i\Delta t$

n = number of samples per 1 circle ($n = 3000$)

T = conscan period ($T = n\Delta t = 60$ s)

ΔT = sliding-window step ($\Delta T < 0.5T$)

$\omega = \dfrac{2\pi}{T}$ (conscan frequency)

$\mu = 4\ln(2) = 2.7726$

r = conscan radius (1.55 mdeg for Ka-band)

h = half-power beamwidth (17 mdeg for Ka-band)

p_i = carrier power at $i\Delta t$

p_o = maximum carrier power

p_m = mean power

v_i = signal noise

$s_i = \begin{Bmatrix} s_{ei} \\ s_{xi} \end{Bmatrix}$ = target position at $i\Delta t$

s_{ei} = elevation component of target position at $i\Delta t$

s_{xi} = cross-elevation component of target position at $i\Delta t$

$\hat{s}_i = \begin{Bmatrix} \hat{s}_{ei} \\ \hat{s}_{xi} \end{Bmatrix}$ = estimated target position at $i\Delta t$

$\hat{s}_{ei}$ = elevation component of the estimated target position at $i\Delta t$

$\hat{s}_{xi}$ = cross-elevation component of the estimated target position at $i\Delta t$

$a_i = \begin{Bmatrix} a_{ei} \\ a_{xi} \end{Bmatrix}$ = antenna position at $i\Delta t$

a_{ei} = elevation component of the antenna position at $i\Delta t$

a_{xi} = cross-elevation component of the antenna position at $i\Delta t$

$e_i = s_i - a_i$ = antenna position error at $i\Delta t$